Editors' Suggestion

Quantum-state reconstruction of unidirectional molecular rotations

Kazuki Ueno,[1] Kenta Mizuse,[1,2] and Yasuhiro Ohshima[1,*]

[1]*Department of Chemistry, School of Science, Tokyo Institute of Technology, 2-12-1-W4-9, Ookayama, Meguro-ku, Tokyo 152-8550, Japan*
[2]*Department of Chemistry, School of Science, Kitasato University, 1-15-1 Kitazato, Minami-ku, Sagamihara 252-0373, Japan*

(Received 13 January 2021; revised 28 March 2021; accepted 14 April 2021; published 5 May 2021)

We present a quantum-state reconstruction procedure to retrieve a rotational wave packet created via nonadiabatic excitation by ultrashort pulses with controlled polarization. Here a unidirectionally rotating ensemble of CO molecules, adiabatically cooled to be populated only in $J = 0$ as an initial state, has been prepared by skewed-polarization pulse-pair excitation. The two-dimensional sections of the molecular-axis probability distribution have been captured by time-delayed Coulomb explosion with the space-slice ion-imaging setup, recently developed in the present research group [K. Mizuse, R. Fujimoto, and Y. Ohshima, Rev. Sci. Instrum. **90**, 103107 (2019)]. The time- and angle-dependent distribution has been subjected to the least-squares regression to provide a unique set of the amplitudes and phases for the eigenstates that constitute the wave packet. The reconstruction allows us to make a movie of the three-dimensional probability distribution and evaluate any physical properties, e.g., the magnitude of rotational angular momentum and its degree of orientation. The determined phases also serve as a sensitive probe for the excitation and the quantum interference to control the directionality of the rotational wave packet.

DOI: 10.1103/PhysRevA.103.053104

I. INTRODUCTION

A microscopic system is fully described by a wave function (WF). Establishing a way to experimentally retrieve WFs is of fundamental interest and also of much significance when the quantum state of the system is exploited for, e.g., information processing [1,2]. For the last two decades, there have been various proposals for such quantum-state reconstruction in atomic and molecular systems [3–7]. Here, a WF to be reconstructed has been regarded as a quantum wave packet (WP), i.e., a time-dependent coherent superposition of several eigenstates of the systems. Since eigenstates constituting a WP are usually well characterized, the reconstruction procedure is recast into the determination of the set of complex expansion coefficients for each eigenstate, or their amplitudes and phases. So far, several studies have reported realization of quantum-state reconstruction of electronic and vibrational WPs [8–13].

Another important objective of the quantum-state reconstruction is molecular rotation. In particular, nonadiabatic (impulsive) excitation by an intense nonresonant ultrashort pulse has been commonly utilized to create a rotational WP in gaseous molecules [14–17]. Molecules in such a nonstationary state exhibit transient alignment along the polarization direction of the excitation pulse, and the resultant anisotropic molecular ensembles in field-free conditions have been extensively utilized to attain detailed information on the geometrical and electronic structure of the molecules [18–20] and to observe electronic and vibrational dynamics in the molecular frame [21–25].

Currently, many researchers are focusing on more sophisticated control of the nonadiabatic molecular alignment by tailoring light fields. In particular, unidirectionally rotating (UDR) molecular WPs have now gained much attention with respect to enantio discrimination for chiral molecules [26–30]. Since the first theoretical consideration and experimental realization [31,32], various approaches have been proposed and demonstrated for creation of UDR-WPs, including a skewed-polarization pulse pair [31,32], a chiral pulse train [33], a polarization-twisted pulse [34–36], and an optical centrifuge [37]. Directionality of the rotational WPs thus created has been determined experimentally by diverse methods, e.g., measurements of circular dichroism [32,33], polarized Raman scattering [37], rotational Doppler effects [34,38], high harmonic generation [35], polarization imaging with vector beams [36], and time-resolved ion imaging [39,40].

Nonadiabatic creation of rotational WPs is so sensitive to the light field because of the highly nonlinear nature of the excitation process. Since precise determination of the light field at the position of the interaction is quite challenging, quantum-state reconstruction of the WPs thus created is crucial. Our research group has developed a reconstruction protocol based on a quantum-state resolved spectroscopic observation, in which the WP created by an ultrashort pulse has been interfered by a delayed replica of the pulse to give delay-dependent change in rotational distribution. Measurements on a finite time sequence of the distribution allow us to retrieve the phases and absolute amplitudes of the WP created by the initial pulse [41]. This approach is, however, incapable to differentiate degenerate eigenstates, i.e., possessing an identical total rotational angular momentum J but different M values of its projection onto the quantization axis. Such degenerate states are inevitably incorporated in rotational WPs created

*ohshima@chem.titech.ac.jp

via polarization-controlled excitation. The other group has also reported rotational WP reconstruction based on the analysis of the degree of alignment measured by, e.g., Coulomb explosion imaging [42]. The method is incapable to apply UDR-WPs either.

Here we report a successful experimental retrieval of a UDR-WP, based on the observation of spatiotemporal propagation of molecular-axis distribution in the laboratory frame. By utilizing the space-slice ion imaging configuration developed in our research group [39,43–45], two-dimensional (2D) sections of the probability distribution, i.e., absolute squares of the WP, have been directly captured as fragment-ion images via time-dependent Coulomb explosion of the UDR molecular ensemble. The time- and angle-dependent distribution thus obtained has been directly fitted to determine the complete set of the amplitudes and phases for the eigenstates constituting the UDR-WP. The present reconstruction procedure can be adopted without any information on the field-matter interaction to create the rotational WP. This is in sharp contrast to the relevant previous studies, where the time-dependent Schrödinger equation (TDSE) was numerically solved with the assumption on the interaction and the laser field parameters were adjusted to simulate the experimental results [39,45,46].

The organization of the paper is as follows. Section II summarizes theoretical fundamentals in creation of rotational WPs via nonadiabatic interaction with ultrashort laser pulses and the spatiotemporal propagation of the probability distribution pertinent to the molecular orientation in space. In Sec. III, the experimental setup adopted in the present paper as well as some details in the experiments are described. In Sec. IV, the time- and angle-dependent probability distribution recorded herein is represented, and the reconstruction procedure is described to determine the amplitudes and phases for the constituent eigenstates in the WPs. In Sec. V, the results presented in the preceding section are discussed with respect to the utilities of the rotational WP reconstruction, in particular, experimentally derived phases as an indispensable probe for the creation mechanism of WPs and quantum interference to control the degree of directionality in UDR-WPs. This is followed by a conclusion in Sec. VI, to mention some outlooks on the rotational WP reconstruction.

II. THEORETICAL BACKGROUND

In the present paper, we have selected a heterodiatomic molecule, carbon monoxide, as a sample to be examined. This is because the molecule is in the nondegenerate $^1\Sigma^+$ electronic ground state, with no nuclear-spin isomers, as opposed to homodiatomic molecules like H_2 and N_2 with ortho- and paramanifolds, and with no hyperfine splitting since the nuclear spins of ^{12}C and ^{16}O are both zero. In addition, the rotational energy intervals of this molecule are relatively large. Thus, as demonstrated later, adiabatic cooling in supersonic expansion essentially makes all the population of the molecules reside in the lowest rotational level with $J = 0$. It allows us to regard the initial molecular ensemble as a pure state and accordingly the quantum state after the interaction with laser fields is fully described with a single wave packet. It is represented as a superposition of rotational eigenstates, $|J, M\rangle$, as

$$\Psi(t) = \sum_{J,M} C_{J,M} \exp(-i\omega_J t)\,|J, M\rangle \tag{1}$$

with J being the quantum number for the total angular momentum $\mathbf{J}$, M the projection of $\mathbf{J}$ onto the space-fixed Z axis, and $C_{J,M}$ the expansion coefficients for $|J, M\rangle$. The coefficient is also represented as $C_{J,M} = A_{J,M}\exp(i\delta_{J,M})$, where $A_{J,M}$ is the amplitude with real and positive value and $\delta_{J,M}$ is the phase angle. $\omega_J = E_J/\hbar$ with $E_J = h[BJ(J+1) - D_J J^2(J+1)^2]$ being the eigenenergy of $|J, M\rangle$, where B and D_J are the rotational and centrifugal-distortion constants (in Hz unit), respectively, of which the values have been precisely known [47]. The coefficients $C_{J,M}$ change in time during the interaction with the laser field and stay constant under field-free conditions. The WP reconstruction is to determine the coefficients for the final state, i.e., after all the field-matter interaction take place.

To create a UDR-WP in CO molecules, we have adopted the skewed-polarization pulse-pair excitation scheme, where the molecular ensemble is interacted with an appropriately delayed pair of two linearly polarized laser pulses of which mutual polarization directions were tilted to each other [31,32]. The space-fixed axes are defined so that the Z axis is along the laser propagation direction [16,32,39]. The polarization directions of the two pulses lie both within the XY plane and here that of the first pulse is defined as along the X axis and that of the second is set tilted by $+45^\circ$ from the X axis (to maximize the directionality) [31,32]. With this axis system, the interaction at time t with the ith pulse ($i = 1$ or 2) is represented as

$$\hat{V}_i(t, \phi_i) = -\frac{E_i(t)^2}{12}\left\{\alpha_\parallel + 2\alpha_\perp - \Delta\alpha D^{(2)*}_{0,0} + \sqrt{\frac{3}{2}}\Delta\alpha\left[D^{(2)*}_{2,0}e^{-2i\phi_i} + D^{(2)*}_{-2,0}e^{+2i\phi_i}\right]\right\} \tag{2}$$

with $E_i(t)$ being the laser pulse envelope, $\alpha_\parallel$ and $\alpha_\perp$ the parallel and perpendicular components of the polarizability, $\Delta\alpha = \alpha_\parallel - \alpha_\perp$, $D^{(k)}_{p,q}$ the Wigner's rotational matrix, and ϕ_i the angle between the X axis and the laser polarization direction ($= 0$ and $\pi/4$ for $i = 1$ and 2, respectively) [16]. If the shapes of the two pulses are identical, the envelope of the second pulse is related to the first one as $E_2(t) \propto E_1(t - \tau)$ with τ being the interval between them. The interaction term in Eq. (2) couples the eigenstates with the change in the quantum numbers as $\Delta J = 0, \pm 2$ and $\Delta M = 0, \pm 2$ [16,48]. This selection rule is identical for Raman transitions but multiple states can be connected via the interaction during a single pulse because of the high strength of the laser field. Then, when the initial state is $|J, M\rangle = |0, 0\rangle$ as is the case in the present paper, the WP thus created as denoted in Eq. (1) is a superposition of eigenstates with $|0, 0\rangle$, $|2, 0\rangle$, $|2, \pm 2\rangle$, $|4, 0\rangle$, $|4, \pm 2\rangle$, $|4, \pm 4\rangle$, and so forth. Even when the shapes and intensities of the two pulses are kept constant, the coefficient $C_{J,M}$ can be manipulated via quantum interference by adjusting the delay τ and the relative polarization direction $\Delta\phi = \phi_1 - \phi_2$ between the pulses.

The rotational eigenfunction of a linear molecule is given as a spherical harmonics: $|J, M\rangle = Y_{J,M}(\theta, \phi) = \Theta_{J,M}(\theta)\Phi_M(\phi)$ with $\Theta_{J,M}(\theta) = N_{J,M}P^M_J(\cos\theta)$ and

$\Phi_M(\phi) = \exp(iM\phi)/\sqrt{2\pi}$ where $P_J^M(x)$ is the associated Legendre polynomial, $N_{J,M}$ is the normalization constant, and θ and ϕ are polar and azimuthal angles [48]. The three-dimensional (3D) spatial distribution concerning the molecular axis in the laboratory frame is represented as the absolute square of the WP, as

$$\begin{aligned} P(\theta,\phi,t) &= |\Psi(\theta,\phi,t)|^2 \\ &= \left| \sum_{J,M} C_{J,M}\Theta_{J,M}(\theta)\Phi_M(\phi)\exp(-i\omega_J t) \right|^2 \\ &= \sum_{J,M} [A_{J,M}\Theta_{J,M}(\theta)]^2/(2\pi) \\ &\quad + \sum_{(J,M)\neq(J',M')} A_{J,M}A_{J',M'}/\pi \\ &\quad \times \Theta_{J,M}(\theta)\Theta_{J',M'}(\theta)\cos(\Delta M\phi - \Delta\omega t + \Delta\delta) \end{aligned} \tag{3}$$

with $\Delta M = M - M'$, $\Delta\omega = \omega_J - \omega_{J'}$, and $\Delta\delta = \delta_{J,M} - \delta_{J',M'}$. All the $C_{J,M}$ coefficients can be determined once the time evolution of the 3D distribution is recorded, but this is extremely challenging. Instead, the time sequence of 2D sections of the distribution, e.g., those in the XY plane (with $\theta = \pi/2$), allows us to retrieve the coefficients when none of $\Theta_{J,M}(\theta)$ vanishes in the configuration. This is the case in the present paper, since $P_J^M(\cos\theta)$ has finite values with $\theta = \pi/2$ when $(J + M)$ is even [48].

III. EXPERIMENT

The experiment was carried out by combining a multipulse optical setup and the space-slice ion-imaging apparatus previously reported [39,43–45].

The schematic of the experimental setup is shown in Fig. 1. Briefly, CO molecules diluted in He (0.15–0.3% with total pressure of 2 MPa) were adiabatically expanded into vacuum and introduced to the interaction region of the imaging apparatus. The rotational temperature of the molecular ensemble was estimated to be 1.5 K, where concentration of the population into $J = 0$ was realized. Then, molecules were irradiated successively by three ultrashort laser pulses coming from a Ti:sapphire laser amplifier. The first and second pulses were for pumping to create a UDR-WP. They were linearly polarized with their center wavelength of 820 nm and the pulse duration of 120 fs. Their intensities were kept relatively low (<70 μJ/pulse with the beam diameter of 28 μm) to avoid unwanted ionization. The polarization of the first pulse was along the X axis while that of the second pulse was tilted by +45° from the axis. The interval of the two pulses was set so that the second pulse hit the molecules at the time when molecules were aligned along the polarization direction of the first pulse. The third pulse was for probing via Coulomb explosion imaging (circularly polarized in the XY plane, 407 nm, 120 fs, >50 μJ/pulse, 8-μm beam diameter). By the irradiation of this pulse, molecules were multiply ionized and then exploded within the laser duration. The angular distribution of fragments in the XY plane was a direct measure of the molecular-axis probability distribution at the time of probe

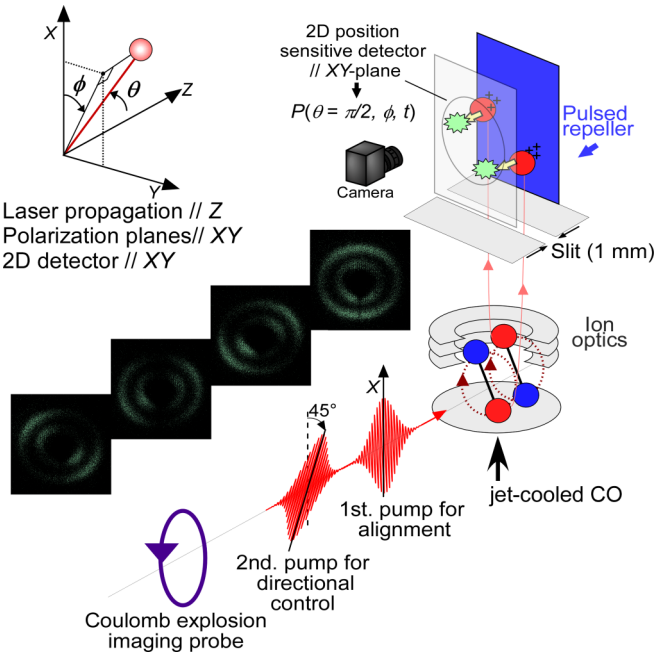

FIG. 1. Schematic of the experimental setup. On the upper-left side, the present space-fixed axis system is shown. Experimentally recorded fragment-ion images at several delay times are also shown in black and white.

irradiation, owing to isotropic ionization efficiency within the plane by the circularly polarized probe pulse. The subsequent UDR-WP dynamics was tracked by scanning the probe delay with a 33- or 67-fs step. The fragment ions thus generated were first accelerated by ion optics to the X direction, and the 3D expanding ion cloud was sliced out to be a 1-mm-thick sheet in the XY plane by passing through a mechanical slit. The sliced sheet of ions of interest was further repelled by applying a pulsed high voltage along the $-Z$ direction to hit the 2D position sensitive detector (microchannel plates backed by a phosphor screen and a digital camera), installed parallel to the XY plane. In the present experiments, ion images of C^{2+} from CO^{3+} or CO^{4+} were measured.

IV. RESULTS AND ANALYSIS

For comparative purposes, we recorded the spatiotemporal evolution of WPs created by a single-pump pulse, as well as UDR-WPs by a pair of pump pulses. Typical examples of the results are shown in Figs. 2 and 3. The figures are false color representations of the time- and angle-dependent probability distributions for single- and double-pump experiments, respectively. Such 2D maps representing wavelike behavior of matter are commonly termed quantum carpets [49]. Figure 2 clearly exhibits a well-known revival structure with the distribution becoming the initial value after every $T_{\rm rev} = 1/(2B) =$ 8.675 ps. Though not so evident, the revival also appears in Fig. 3. The quantum carpet for the single pump is symmetric with respect to the horizontal line at $\phi = 180°$, while that for the double pump shows traces at an angle. This is a signature of directional rotation (clockwise in this case), with the ϕ angle increasing with time. The alignment parameters $\langle\cos^2\phi\rangle$

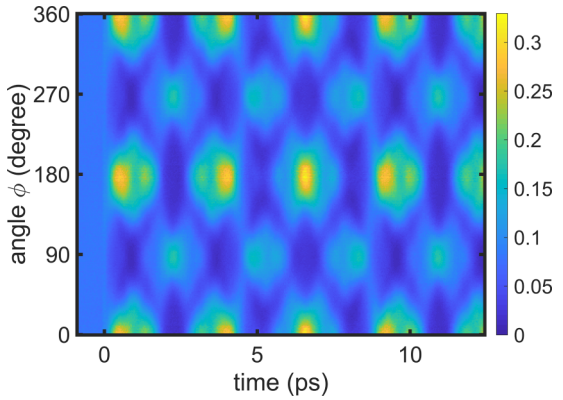

FIG. 2. Time- and angle-dependent probability distribution for a rotational WP created by a single-pump pulse. The horizontal axis corresponds to delay time of the probe pulse relative to the pump pulse, and the vertical axis corresponds to the azimuthal angle ϕ. The pump intensity was estimated to be ≈15 TW/cm^2. The polarization direction of the pump pulse is directed along $\phi = 0$ and 180°.

for the two carpets are shown in Fig. 4, to assess the degree of alignment and its temporal dynamics.

The distribution is periodic both in time and angle, as represented in Eq. (3). Thus beat components for sets of $(\Delta\omega, \Delta M)$ can be extracted by 2D Fourier transformation. The results for the single- and double-pump experiments are shown in Figs. 5 and 6, respectively. Here the 2D power spectra developed in the $\Delta\omega$ and ΔM domains are shown in false color representation. The maximum beat frequency observed in the $\Delta\omega$ domain is $20B$ both in Figs. 5 and 6. This value is for $J = 4 \leftrightarrow 0$ and thus the two rotational WPs are composed of the eigenstates with $J = 0$, 2, and 4. In addition, there is no appreciable peak at $10B$ for $J = 3 \leftrightarrow 1$. This observation confirms that contribution of WPs from the $J = 1$ initial state is negligible. The compositions of the peaks in the 2D power spectrum are different to each other. The

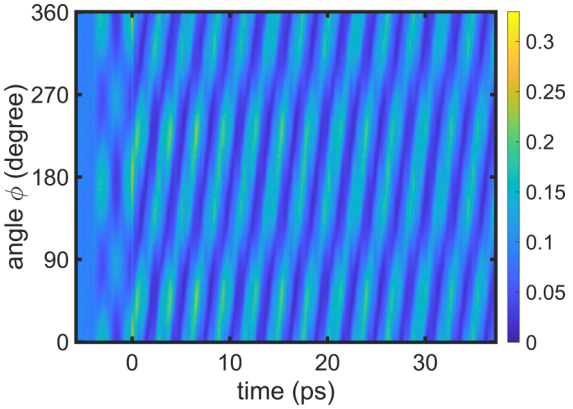

FIG. 3. Time- and angle-dependent probability distribution for a UDR-WP created by a skewed-polarization pair of pump pulses. Time zero is set to the peak of the second pulse. The first pulse was introduced 3.87 ps before. The pulse intensities were estimated to be 6 TW/cm^2 or more. The polarization direction of the first pump pulse is directed along $\phi = 0$ and 180° while that of the second pump is tilted by +45°.

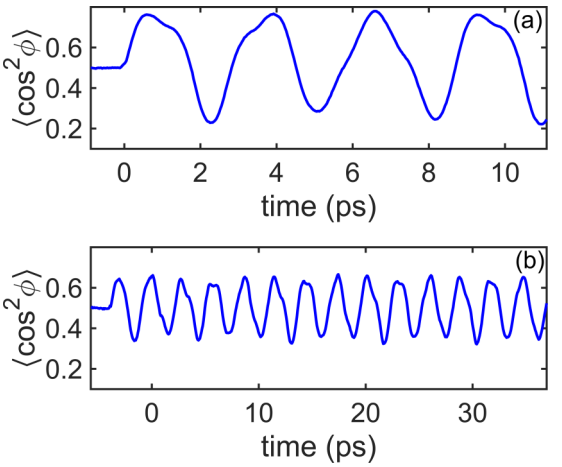

FIG. 4. Time-dependent alignment parameters $\langle\cos^2\phi\rangle$ for (a) the rotational WP created by a single-pump pulse (corresponding to Fig. 2) and (b) the UDR-WP created by a skewed-polarization pair of pump pulses (corresponding to Fig. 3).

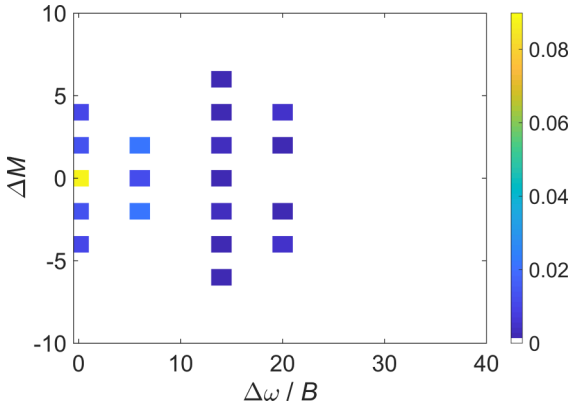

FIG. 5. Power spectrum from the 2D Fourier transformation of the time- and angle-dependent probability distribution (shown in Fig. 2) from the single-pump experiment. The horizontal axis corresponds to the frequency in the B unit and the vertical axis corresponds to the M quantum number.

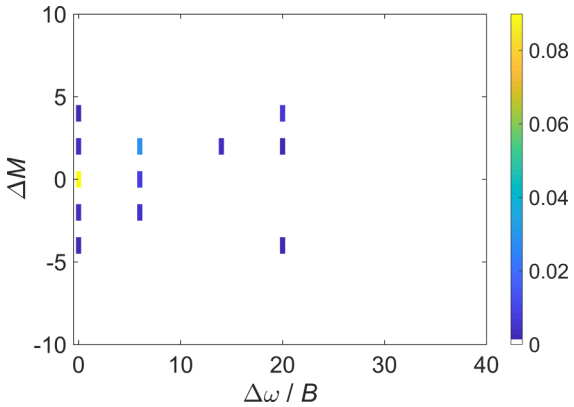

FIG. 6. Power spectrum from the 2D Fourier transformation of the time- and angle-dependent probability distribution (shown in Fig. 3) from the double-pump experiment. Note the frequency resolution is four times better than in Fig. 5 due to the extended coverage in time.

peak at $(\Delta\omega, \Delta M) = (6B, 2)$ contains only a single component of $|2, 2\rangle \leftrightarrow |0, 0\rangle$. On the other hand, the peak at (0,2) includes six components: $|4, -2\rangle \leftrightarrow |4, -4\rangle$, $|4, 0\rangle \leftrightarrow |4, -2\rangle$, $|4, 2\rangle \leftrightarrow |4, 0\rangle$, $|4, 4\rangle \leftrightarrow |4, 2\rangle$, $|2, 2\rangle \leftrightarrow |2, 0\rangle$, and $|2, 0\rangle \leftrightarrow |2, -2\rangle$. It is noted that the peaks at (0,2) and $(0, -2)$ are complex conjugate to each other, and their information contents are essentially the same.

The gross feature of the 2D power spectrum visualizes the nature of the rotational WP. In Fig. 5, the magnitudes of the peaks at $+\Delta M$ and $-\Delta M$ are essentially identical for the same $\Delta\omega$. This directly indicates that the net value of ΔM is vanishing, consequently $\langle \hat{J}_Z \rangle = 0$ for the rotational WP created by a linearly polarized pulse. On the other hand, peaks with positive ΔM's dominate over those with negative values in Fig. 6. This is a clear manifestation of the positively oriented rotational angular momentum in the WP created via the skewed-polarization pulse-pair excitation.

Since the time- and angle-dependent probability distribution is represented as Eq. (3), real and imaginary components of each peak in the 2D Fourier-transformed spectrum of the distribution are given as

$$\mathrm{Re}(\Delta\omega, \Delta M) = \sum \Theta_{J,M}(\pi/2)\Theta_{J',M'}(\pi/2)/\pi \times A_{J,M}A_{J',M'} \cos(\delta_{J,M} - \delta_{J',M'}) \quad (4)$$

and

$$\mathrm{Im}(\Delta\omega, \Delta M) = \sum \Theta_{J,M}(\pi/2)\Theta_{J',M'}(\pi/2)/\pi \times A_{J,M}A_{J',M'} \sin(\delta_{J,M} - \delta_{J',M'}), \quad (5)$$

respectively, where the summation is taken over J, J', M, and M' that satisfy $\Delta\omega = \omega_J - \omega_{J'}$ and $\Delta M = M - M'$. It implies that the amplitudes $A_{J,M}$ and phases $\delta_{J,M}$ for the eigenstates that constitute the rotational WP can be determined from the data set of the peaks in Fourier space, as given in Eqs. (4) and (5). Then we employed the Gerchberg-Saxton algorithm for the retrieval of the amplitudes and phases [50]. Unfortunately, the determined parameters accompany with relatively large uncertainty. In particular, the standard deviations for the phases are close to 50° for the worst case. This inferior quality of the fit may be mostly due to the determination of many parameters (18 in total) from limiting numbers (at most 20) of the peaks in the Fourier space. So we finally executed direct least-squares fitting of the quantum carpets shown in Figs. 2 and 3 to the function in angle ϕ and time t represented as Eq. (3) with θ fixed to $\pi/2$, to determine the set of $A_{J,M}$ and $\delta_{J,M}$. Here the set of the amplitudes derived from the fit of the peaks in the power spectra was used as initial values. The amplitudes and phases thus determined are shown in Figs. 7 and 8 for the single-pulse excitation while those for the skewed-polarization pulse-pair excitation are shown in Figs. 9 and 10. Since the differences between the phases are only determined as shown in Eq. (3), the value of $\delta_{0,0}$ is arbitrarily fixed to zero. As expected, the amplitudes of $\pm M$ with the same J values are identical for the former WP, while those for the latter, i.e., UDR-WP, exhibits predominance for positive M values. The values of the phase angles determined show characteristic trends. For the single-pulse excitation, the phases of $\pm M$ with the same J are essentially identical, and they show $+180°$ shift by $\Delta M = \pm 2$. On the other hand, the phases in the UDR-WP do not exhibit such regular changes. The interpretation of the characteristics will be discussed later.

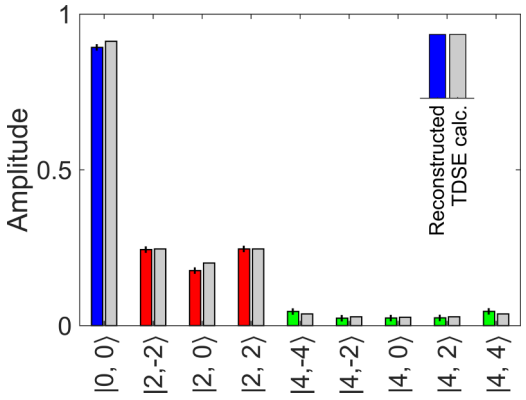

FIG. 7. A bar diagram representing the amplitudes $A_{J,M}$ of the rotational eigenstates $|J, M\rangle$ that constitute the rotational WP created by the single-pulse excitation. The horizontal axis is for the rotational states and the vertical axis is for the magnitudes of the amplitude. Colored bars on the left side for each $|J, M\rangle$ are those determined by the least-squares regression on the time- and angle-dependent probability distribution shown in Fig. 2. The error bars for the standard deviations of the fit are indicated. Gray bars on the right side are those derived from the TDSE calculation, in which the laser pulse with Gaussian envelope (120-fs duration, 11-TW/cm^2 peak power) is adopted.

To demonstrate the agreement between the observation and the reconstructed results, movies of the 2D representation of the time- and angle-dependent probability distribution are given as Supplemental Material (Movies S1 and S2 for the single-pulse and skewed-polarization pulse-pair excitation, respectively) [51]. Several snapshots of the observed and reconstructed 2D probability distributions are also represented in Fig. 11 for the UDR-WP.

To confirm the experimentally reconstructed sets of the amplitudes and phases of the rotational WPs, we also performed TDSE calculation [16] by adopting appropriate parameters for the ultrashort pump pulses and the molecular constants of CO

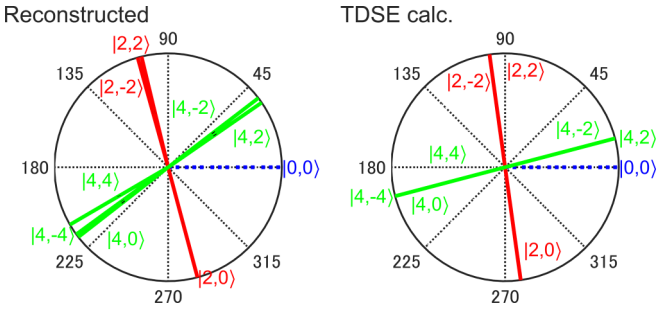

FIG. 8. A polar plots representing the phase angles $\delta_{J,M}$ of the rotational eigenstates $|J, M\rangle$ that constitute the rotational WP created by the single-pulse excitation. The value for the $|0, 0\rangle$ state is fixed to zero. Left: Those determined by the least-squares regression on the time- and angle-dependent probability distribution shown in Fig. 2. The error bars for the standard deviations of the fit are buried within the thickness of the lines. Right: Those derived from the TDSE calculation.

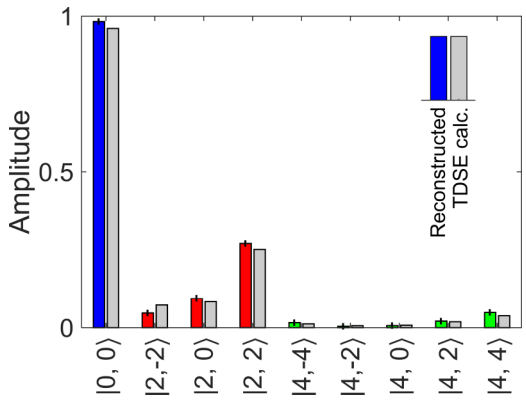

FIG. 9. A bar diagram representing the amplitudes $A_{J,M}$ of the rotational eigenstates $|J, M\rangle$ that constitute the rotational WP created by the skewed-polarization pulse-pair excitation. Colored bars on the left side for each $|J, M\rangle$ are those determined by the least-squares regression on the time- and angle-dependent probability distribution shown in Fig. 3. Gray bars on the right side are those derived from the TDSE calculation, in which the laser pulses with Gaussian envelope (120-fs duration, 5.3 and 5.5 TW/cm^2 for the first and second pulses) are adopted. The time interval between the two pump pulses is set to be 3.87 ps.

[47,52]. The results are also shown in Figs. 7–10. The TDSE results satisfactorily agree with the reconstructed amplitudes and phases, once the peak powers of the pump pulses are adjusted. The agreement validates the present reconstruction of the rotational WPs. The peak powers to give good match-up with the reconstruction results are slightly smaller than those estimated from the experimental pulse parameters.

V. DISCUSSION

In the present paper, the amplitudes and phases for the eigenstates constituting the WPs have been precisely determined, and thus the time evolution of the WPs can be fully reconstructed in 3D space. The molecular movies thus derived for the probability distribution are given in the Supplemental Material [51]. As it must be, the 3D time-dependent distribution for the single-pulse excitation exhibits alignment

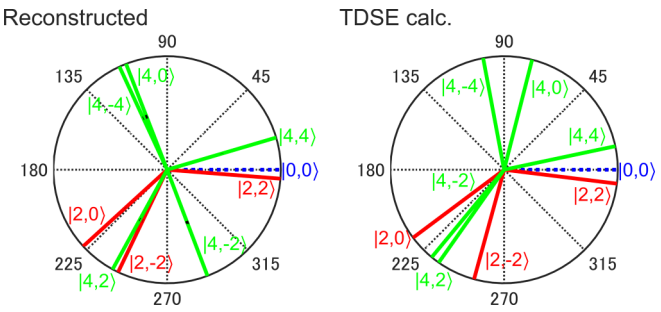

FIG. 10. A polar plots representing the phase angles $\delta_{J,M}$ of the rotational eigenstates $|J, M\rangle$ that constitute the rotational WP created by the skewed-polarization pulse-pair excitation. Left: Those determined by the least-squares regression on the time- and angle-dependent probability distribution shown in Fig. 3. Right: Those derived from the TDSE calculation.

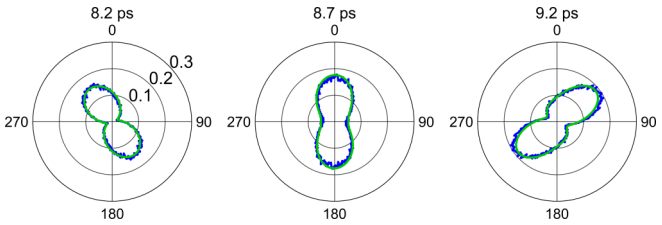

FIG. 11. Snapshots of the observed (blue or dark gray line) and reconstructed (green or light gray line) 2D probability distribution for the UDR-WP at several delay times. The distribution is indicated in the polar plots for the ϕ angle.

dynamics with axial symmetry around the polarization vector (the X axis) as shown in Movie S3. Movie S4 demonstrates unidirectionally rotating dynamics induced by the skewed-polarization pulse-pair excitation. Since the WP thus created is composed of almost exclusively the $J = 0$ and 2 states, with negligible contribution (0.3% in population) from $J = 4$, it exhibits almost nondispersing spatiotemporal propagation, i.e., the shape of the 3D distribution shows marginal modification while keeping UDR, as has been discussed in the previous studies [53,54]. Characterization of 3D probability distribution is indispensable when the anisotropic molecular ensemble in the nonstationary quantum state is utilized for detailed studies on photoexcitation dynamics of molecules and manipulation of waveforms and polarization of optical fields. Also, any physical quantity can be evaluated from the reconstructed WPs. For the rotational WP created by the single-pulse excitation, $\langle\hat{\mathbf{J}}^2\rangle$ and $\langle\hat{J}_Z\rangle$ are evaluated to be 1.03 and 0.0, respectively, and those for the UDR-WP by the skewed-polarization pulse-pair excitation are 0.59 and 0.16.

The characteristics in the phases here determined are interpreted as follows. As shown by the predominance of $|J, M\rangle = |0, 0\rangle$ ($\geqslant$80% in population), the excitation by the ultrashort pulses in the present paper is so weak that the coefficients for $J = 2$ are well evaluated by the first-order perturbation. In the infinitesimally short pulse limit, the coefficients by the ith pulse are approximated as

$$C^{(i)}_{2,M} = \frac{1}{i\hbar}\int \langle 2, M|\,\hat{V}_i(t,\phi_i)\,|0,0\rangle \exp(i\omega_J t)dt$$
$$\approx -\frac{i}{12\hbar}\Delta\alpha F_{2,M}(\phi_i)\int [E_i(t)]^2 dt \qquad (6)$$

with

$$F_{2,M}(\phi_i) = \begin{cases} \langle 2,0|D^{(2)*}_{0,0}|0,0\rangle & M = 0 \\ -\sqrt{\frac{3}{2}}e^{-2i\phi_i}\langle 2,2|D^{(2)*}_{2,0}|0,0\rangle & M = +2 \\ -\sqrt{\frac{3}{2}}e^{+2i\phi_i}\langle 2,-2|D^{(2)*}_{-2,0}|0,0\rangle & M = -2 \end{cases}. \qquad (7)$$

For the single-pulse excitation, $\phi_i = 0$ and thus the phase factors are estimated as $-i$ for $M = 0$ while $+i$ for $M = \pm 2$, since $\Delta\alpha > 0$ and the matrix elements of $D^{(2)*}_{M,0}$ are real and positive. The involvement of the states with $J = 4$ proceeds via two-step Raman excitations: $J = 0 \to 2 \to 4$. Therefore, the phases of $J = 4$ are further shifted by -90° and $+90^\circ$ for $\Delta M = 0$ and ± 2, respectively, from those of $J = 2$. This simple consideration reasonably agrees with the reconstructed

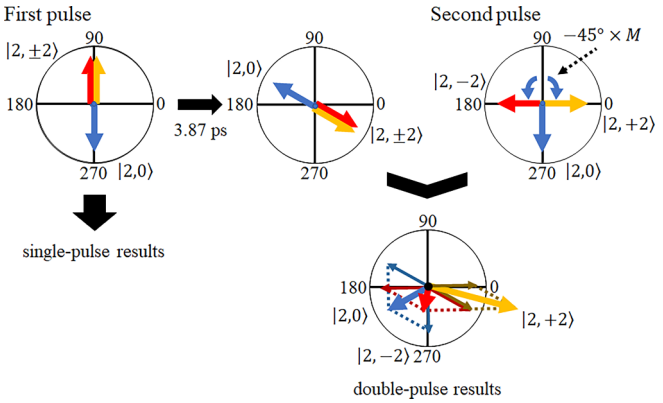

FIG. 12. Schematic representation of complex coefficients in the skewed-polarization pulse-pair excitation. The coefficients of $J = 2$ are indicated as arrows (blue, $M = 0$; orange, $M = +2$; red, $M = -2$) in the complex plane (real and imaginary parts in the horizontal and vertical axes, respectively). The two plots in the upper left represent the creation of the WP by the first pulse and its time evolution. The plot in the upper right is for the WP creation by the second pulse. The vectorial addition of the two coefficients yields to the final states, represented in the lower plot.

results shown in Fig. 8. Slight offsets from the estimation may originate from effects of the finite pulse width.

The situation in the double-pulse excitation is more involved. Schematic representation is shown in Fig. 12. Here the final coefficient is approximated as a simple sum of those by the two pulses given in Eq. (6) since the excitation is executed under weak-field conditions. Then the phases by the first pulse are estimated to be -90° and $+90^\circ$ for $M = 0$ and ± 2 in $J = 2$, respectively, as discussed above. Due to the delay ($\tau = 3.87$ ps) to the second pulse, the WP created by the first pulse exhibits time evolution and the phases of the state with $J = 2$ are rotated by the angle of $-\omega_{J=2}\tau = -480^\circ (= -120^\circ)$. The WP created by the second pulse has different initial phases (180° for $M = +2$ and zero for $M = -2$) due to the skewed angle of the polarization $\phi_2 = 45^\circ$ [see Eq. (7)]. The complex coefficients for the two pulses are summed up to be the final ones, as shown in Fig. 12. Since the coefficients by the two pulses are almost parallel to each other for $M = +2$ while those for $M = -2$ point to opposite directions, the resultant amplitude for $M = +2$ much dominates over that for $M = -2$, to give a large degree of orientation in final WP. This simple model reasonably reproduces the reconstructed results shown in Figs. 9 and 10. This exemplifies the utility of experimentally reconstructed results, in particular phases, to serve as a sensitive probe for the excitation process to create the rotational WP. It is noted that the phase shift $-\omega_{J=2}\tau$ due to the waiting time has not been set here exactly to -90°, to give a favorable condition also to the contribution from states with $J = 4$. The pulse interval dependence of the degree of orientation has been discussed in some detail in our recent study [45].

VI. CONCLUSION

In the present paper, we demonstrate the quantum-state reconstruction of the rotational WPs by utilizing time-resolved ion imaging coupled with the skewed-polarization pulse-pair excitation for the creation of the UDR molecular ensemble. The key to this successful demonstration is the implementation of the space-slice ion-imaging experimental setup developed by our research group [39,43–45]. It allows us to directly capture the time- and angle-dependent probability distribution in the plane perpendicular to the laser propagation direction with 2D isotropic detection efficiency by using the circularly polarized Coulomb explosion probe pulse. The time sequences of the probability distribution thus recorded precisely are subjected to the least-squares regression to determine the unique sets of the amplitudes and phases of eigenstates constituting the WPs. Then, the WPs are fully retrieved, to track the spatiotemporal evolution of the 3D probability distribution, and to evaluate any physical properties, i.e., the expectation values of the angular momentum and its degree of orientation. In particular, the reconstructed phases are indispensable experimental sources to shed light on the excitation processes to create WPs. In the present paper, the WP creation is in the perturbative regime with weak-field excitation. It is expected that the phases exhibit substantial deviation from those in the weak-field limit when the excitation pulse becomes stronger [41]. Such nonperturbative signature will be captured in UDR-WPs by applying the method presented here to experiments with more intense excitation pulses.

We will finally make some discussion on possible applicability of the present WP reconstruction to molecular systems other than heterodiatomic molecules, such as symmetric- and asymmetric-top molecules. The discussion is very relevant to the topic mentioned in the Introduction, namely, UDR of chiral molecules to be utilized for enantio discrimination [26–30]. Achieving a higher degree of rotational angular momentum orientation is crucial for increasing the discrimination efficiency. To this end, experimental evaluation of the orientation is important and WP reconstruction may contribute to a considerable extent.

When a rotational WP is created from a single initial state in a symmetric- or asymmetric-top molecule, the time-dependent spatial distribution is represented with a functional form similar to Eq. (3), where the angular parts $\Theta_{J,M}(\theta)$ should only be replaced by appropriate functions. Thus, the rotational WP can be reconstructed by the present protocol, unless the plane of detection is coincident with a nodal plane of eigenfunctions that constitute the WP. In case of polyatomic molecules, rotational states are more congested than diatomic molecules. Even by adopting extensive adiabatic cooling, it is hardly realized to concentrate the rotational-state distribution of the sample into the lowest $J = 0$ state. In this respect, utilization of the Stark deflector to spatially separate quantum states of polar molecules will be very beneficial [46,55]. When the initial molecular ensemble is in an incoherent manner, e.g., a thermal ensemble with finite temperature, the system is fully described by a density matrix. Complete retrieval of the density matrix should be too demanding, since information encoded in 2D time-dependent angular probability is generally insufficient to independently determine all the matrix elements. Even in this case, the method developed in the present paper will be of some use. In particular, 2D Fourier transformation analysis on the time-dependent

angular probability will visualize the composition of the rotational WPs, as exemplified in Figs. 5 and 6.

Another issue to be addressed is to correctly image the probability distribution via Coulomb explosion or photodissociation of polyatomic molecules. Ionization and dissociation dynamics of this kind of molecules are much involved and axial-recoil approximation for fragments may not be valid. The deconvolution of the nonaxial-recoil effects in a Coulomb explosion has been reported [56]. Such a detailed consideration will be valuable for UDR-WP reconstruction of polyatomic molecules including chiral species.

ACKNOWLEDGMENTS

The work was partly supported by grants-in-aid from Ministry of Education, Culture, Sports, Science and Technology, Japan (Grants No. 22245004, No. 26620020, No. 15H03766, No. 15KT0060, No. 16K13927, No. 18H03897, No. 18J21311, No. 19K22164, and No. 20K21169), Consortium for Photon Science and Technology, the Shimadzu Science Foundation, the Harmonic Ito Foundation, and the Fujikura Foundation. K.U. acknowledges the financial support from Japan Society for the Promotion of Science Research Fellowships for Young Scientists.

[1] J. A. Cina, Annu. Rev. Phys. Chem. **59**, 319 (2008).
[2] K. Ohmori, Annu. Rev. Phys. Chem. **60**, 487 (2009).
[3] M. Shapiro, J. Chem. Phys. **103**, 1748 (1995).
[4] X. Chen and J. A. Yeazell, Phys. Rev. A **56**, 2316 (1997).
[5] I. S. Averbukh, M. Shapiro, C. Leichtle, and W. P. Schleich, Phys. Rev. A **59**, 2163 (1999).
[6] A. S. Mouritzen and K. Mølmer, J. Chem. Phys. **124**, 244311 (2006).
[7] S. Ramakrishna and T. Seideman, Phys. Rev. A **87**, 023411 (2013).
[8] T. J. Dunn, I. A. Walmsley, and S. Mukamel, Phys. Rev. Lett. **74**, 884 (1995).
[9] T. C. Weinacht, J. Ahn, and P. H. Bucksbaum, Phys. Rev. Lett. **80**, 5508 (1998).
[10] E. Skovsen, H. Stapelfeldt, S. Juhl, and K. Mølmer, Phys. Rev. Lett. **91**, 090406 (2003).
[11] A. Monmayrant, B. Chatel, and B. Girard, Phys. Rev. Lett. **96**, 103002 (2006).
[12] P. F. Tekavec, T. R. Dyke, and A. H. Marcus, J. Chem. Phys. **125**, 194303 (2006).
[13] Y. Nabekawa, Y. Furukawa, T. Okino, A. Amani Eilanlou, E. J. Takahashi, K. Yamanouchi, and K. Midorikawa, Nat. Commun. **6**, 8197 (2015).
[14] H. Stapelfeldt and T. Seideman, Rev. Mod. Phys. **75**, 543 (2003).
[15] T. Seideman and E. Hamilton, Adv. Atom. Mol. Opt. Phys. **52**, 289 (2005).
[16] Y. Ohshima and H. Hasegawa, Int. Rev. Phys. Chem. **29**, 619 (2010).
[17] C. P. Koch, M. Lemeshko, and D. Sugny, Rev. Mod. Phys. **91**, 035005 (2019).
[18] J. Itatani, J. Levesque, D. Zeidler, H. Niikura, H. Pepin, J. C. Kieffer, P. B. Corkum, and D. M. Villeneuve, Nature (London) **432**, 867 (2004).
[19] T. Kanai, S. Minemoto, and H. Sakai, Nature (London) **435**, 470 (2005).
[20] J. Yang, J. Beck, C. J. Uiterwaal, and M. Centurion, Nat. Commun. **6**, 8172 (2015).
[21] D. Pavičić, K. F. Lee, D. M. Rayner, P. B. Corkum, and D. M. Villeneuve, Phys. Rev. Lett. **98**, 243001 (2007).
[22] J. L. Hansen, H. Stapelfeldt, D. Dimitrovski, M. Abu-samha, C. P. J. Martiny, and L. B. Madsen, Phys. Rev. Lett. **106**, 073001 (2011).
[23] J. B. Bertrand, H. J. Wörner, P. Salières, D. M. Villeneuve, and P. B. Corkum, Nat. Phys. **9**, 174 (2013).
[24] P. M. Kraus, B. Mignolet, D. Baykusheva, A. Rupenyan, L. Horn, E. F. Penka, G. Grassi, O. I. Tolstikhin, J. Schneider, F. Jensen, L. B. Madsen, A. D. Bandrauk, and F. R. H. J. Wörner, Science **350**, 790 (2015).
[25] Y. Mi, P. Peng, N. Camus, X. Sun, P. Fross, D. Martinez, Z. Dube, P. B. Corkum, D. M. Villeneuve, A. Staudte, R. Moshammer, and T. Pfeifer, Phys. Rev. Lett. **125**, 173201 (2020).
[26] A. Yachmenev and S. N. Yurchenko, Phys. Rev. Lett. **117**, 033001 (2016).
[27] I. Tutunnikov, E. Gershnabel, S. Gold, and I. S. Averbukh, J. Phys. Chem. Lett. **9**, 1105 (2017).
[28] A. A. Milner, J. A. M. Fordyce, I. MacPhail-Bartley, W. Wasserman, V. Milner, I. Tutunnikov, and I. S. Averbukh, Phys. Rev. Lett. **122**, 223201 (2019).
[29] A. Yachmenev, J. Onvlee, E. Zak, A. Owens, and J. Küpper, Phys. Rev. Lett. **123**, 243202 (2019).
[30] I. Tutunnikov, J. Floß, E. Gershnabel, P. Brumer, I. S. Averbukh, A. A. Milner, and V. Milner, Phys. Rev. A **101**, 021403(R) (2020).
[31] S. Fleischer, Y. Khodorkovsky, Y. Prior, and I. S. Averbukh, New J. Phys. **11**, 105039 (2009).
[32] K. Kitano, H. Hasegawa, and Y. Ohshima, Phys. Rev. Lett. **103**, 223002 (2009).
[33] S. Zhdanovich, A. A. Milner, C. Bloomquist, J. Floß, I. S. Averbukh, J. W. Hepburn, and V. Milner, Phy. Rev. Lett. **107**, 243004 (2011).
[34] G. Karras, M. Ndong, E. Hertz, D. Sugny, F. Billard, B. Lavorel, and O. Faucher, Phys. Rev. Lett. **114**, 103001 (2015).
[35] O. Faucher, E. Prost, E. Hertz, F. Billard, B. Lavorel, A. A. Milner, V. A. Milner, J. Zyss, and I. S. Averbukh, Phys. Rev. A **94**, 051402(R) (2016).
[36] J. Bert, E. Prost, I. Tutunnikov, P. Béjot, E. Hertz, F. Billard, B. Lavorel, U. Steinitz, I. S. Averbukh, and O. Faucher, Laser Photon. Rev. **14**, 1900344 (2020).
[37] A. Korobenko, A. A. Milner, and V. Milner, Phys. Rev. Lett. **112**, 113004 (2014).
[38] O. Korech, U. Steinitz, R. J. Gordon, I. S. Averbukh, and Y. Prior, Nat. Photon. **7**, 711 (2013).
[39] K. Mizuse, K. Kitano, H. Hasegawa, and Y. Ohshima, Sci. Adv. **1**, e1400185 (2015).

[40] K. Lin, Q. Song, X. Gong, Q. Ji, H. Pan, J. Ding, H. Zeng, and J. Wu, Phys. Rev. A **92**, 013410 (2015).
[41] H. Hasegawa and Y. Ohshima, Phys. Rev. Lett. **101**, 053002 (2008).
[42] A. A. Søndergaard, B. Shepperson, and H. Stapelfeldt, J. Chem. Phys. **147**, 013905 (2017).
[43] K. Mizuse, R. Fujimoto, N. Mizutani, and Y. Ohshima, J. Vis. Exp. **120**, e54917 (2017).
[44] K. Mizuse, R. Fujimoto, and Y. Ohshima, Rev. Sci. Instrum. **90**, 103107 (2019).
[45] K. Mizuse, N. Sakamoto, R. Fujimoto, and Y. Ohshima, Phys. Chem. Chem. Phys. **22**, 10853 (2020).
[46] E. T. Karamatskos, S. Raabe, T. Mullins, A. Trabattoni, P. Stammer, G. Goldsztejn, R. R. Johansen, K. Dlugolecki, H. Stapelfeldt, M. Vrakking, S. Trippel, A. Rouzee, and J. Küpper, Nat. Commun. **10**, 3364 (2019).
[47] I. Nolt, J. Radostitz, G. DiLonardo, K. Evenson, D. Jennings, K. Leopold, M. Vanek, L. Zink, A. Hinz, and K. Chance, J. Mol. Spectrosc. **125**, 274 (1987).
[48] R. N. Zare, *Angular Momentum: Understanding Spatial Aspects in Chemistry and Physics* (Wiley, New York, 1988).
[49] A. E. Kaplan, I. Marzoli, W. E. Lamb, and W. P. Schleich, Phys. Rev. A **61**, 032101 (2000).
[50] R. W. Gerchberg and W. O. Saxton, Optik **35**, 237 (1972).
[51] See Supplemental Material at http://link.aps.org/supplemental/10.1103/PhysRevA.103.053104 for the 2D and 3D representation of the time- and angle-dependent probability distribution for the single-pulse and skewed-polarization pulse-pair excitation (Movies S1–S4).
[52] M. P. Bogaard, A. D. Buckingham, R. K. Pierens, and A. White, J. Chem. Soc., Faraday Trans. 1 **74**, 3008 (1978).
[53] J. P. Cryan, J. M. Glownia, D. W. Broege, Y. Ma, and P. H. Bucksbaum, Phys. Rev. X **1**, 011002 (2011).
[54] A. Korobenko, J. W. Hepburn, and V. Milner, Phys. Chem. Chem. Phys. **17**, 951 (2015).
[55] A. Trabattoni, J. Wiese, U. D. Giovannini, J.-F. Olivieri, T. Mullins, J. Onvlee, S.-K. Son, B. Frusteri, A. Rubio, S. Trippel, and J. Küpper, Nat. Commun. **11**, 2546 (2020).
[56] L. Christensen, L. Christiansen, B. Shepperson, and H. Stapelfeldt, Phys. Rev. A **94**, 023410 (2016).